

Updated and Projected Cosmic Microwave Background Bounds on WIMP Annihilation

Charlotte Myers

MIT Department of Physics, 77 Massachusetts Ave., Cambridge, MA 02139, USA

Dominic Agius

Instituto de Física Corpuscular (IFIC), CSIC-Universitat de València, 46071, Valencia, Spain

Daniele Gaggero

INFN Sezione di Pisa, Polo Fibonacci, Largo B. Pontecorvo 3, 56127 Pisa, Italy

Angelo Ricciardone

Dipartimento di Fisica “Enrico Fermi”, Università di Pisa,

Largo Bruno Pontecorvo 3, Pisa I-56127, Italy and

INFN Sezione di Pisa, Polo Fibonacci, Largo B. Pontecorvo 3, 56127 Pisa, Italy

(Dated: December 12, 2025)

We derive updated Cosmic Microwave Background (CMB) constraints on annihilating dark matter, and present forecasts for upcoming CMB surveys. We show that the addition of recent temperature, polarization, and lensing data from ground-based experiments yields only minor improvements ($\approx 10\%$) compared to Planck bounds, confirming that the sensitivity remains dominated by the large-scale E-mode polarization. Forecasts, using a LiteBIRD-like setup, indicate that pairing a low-noise, wide-sky satellite at $\ell < 200$ with high-resolution ground observations nearly saturates the cosmic-variance limit, improving bounds by $\approx 60\%$, where our derived 95th percentile limit is $p_{\text{ann}} < 1.27 \times 10^{-28} \text{ cm}^3 \text{ s}^{-1} \text{ GeV}^{-1}$. We also consider the inclusion of B-mode polarization for a realistic future experiment.

I. INTRODUCTION

The Weakly Interacting Massive Particle (WIMP) paradigm remains one of the most widely studied and theoretically well-motivated dark matter (DM) scenarios [1]. Within this framework, the generic prediction of DM annihilation into Standard Model particles implies an energy injection that alters the thermal and ionization history of the universe. This impact is measurable during the cosmic dark ages—the period between recombination and reionization—when the intergalactic medium is otherwise nearly neutral and astrophysical sources are absent. Through an exotic electromagnetic injection, annihilating DM leaves a distinct imprint on the cosmic microwave background (CMB) by increasing the free-electron abundance and enhancing Thomson scattering with CMB photons, thereby modifying the Thomson optical depth. This indirect observation channel has been studied in detail, leading to some of the most stringent constraints on DM annihilation [2–22].

With the advent of precision cosmology, it became possible to constrain the DM annihilation cross section using CMB polarization data [3]. This effort built on earlier works examining the impact of decaying DM on the recombination history and the resulting CMB signatures [23–28]. Subsequent studies refined these analyses by developing increasingly accurate treatments of energy injection and deposition during the dark ages [4, 5]. In these studies, it was recognized that the bulk of the constraining power, when considering changes to the Thomson optical depth induced from additional ionizations

from DM annihilation, comes from large angular scales, with sensitivity dominated by the low-multipole polarization [3, 15, 29]. This emphasis on low- ℓ E-mode polarization, and the corresponding insensitivity of small-scale TT data, once parameter degeneracies are marginalized, was sharpened in later analyses, which also clarified why polarization systematically outperforms temperature measurements for energy injection constraints [30]. In parallel, several forecast studies compared the capability of Planck with those of cosmic-variance-limited (CVL) and ground-based experiments [29, 31, 32]. Subsequent work further identified the redshift ranges and multipole scales most relevant for DM-induced energy deposition, providing a unified framework for understanding how the deposition history maps onto CMB observables [33].

Amid this progress, forecasts for next generation high-resolution, ground-based CMB experiments, such as CMB-S4 [34], indicated substantial improvements over Planck in their ability to constrain DM energy injection [15, 31, 35]. While Ref. [15] anticipated moderate improvements from CMB-S4 over Planck, Refs. [31, 35] initially claimed an order-of-magnitude improvement. However, the latter estimate was later revised, indicating a more modest enhancement of only a factor of ~ 2 [36]. This reinforced the general consensus that, once low- ℓ large-scale polarization is constrained, additional high- ℓ sensitivity yields only marginal improvements. Recent forecasts including a LiteBIRD-like satellite reinforce this picture: combining space-based, low-noise E-mode polarization at $\ell \lesssim 100$ with high-resolution ground-based data effectively saturates the information available from

the CMB and approaches the cosmic-variance limit for realistic sky coverage [37]. In this work, we revisit current bounds in the post-Planck era using updated ACT, SPT, and DESI measurements. We also present forecasts that explicitly quantify where the information resides in multipole space and how close future survey combinations can come to the CVL floor. Moreover, we also consider the phenomenological imprint on B -mode polarization data.

The rest of this paper is organized as follows. In Sec. II we review how DM annihilation modifies the ionization history and CMB anisotropies, introduce the parameter p_{ann} , and quantify the multipole ranges that drive the constraining power using Fisher forecasts. In Sec. III we update current limits on p_{ann} by combining Planck with recent ACT and SPT data, as well as BAO data, and examine the resulting parameter degeneracies. Sec. IV presents forecasts for future CMB configurations, including LiteBIRD- and CMB-S4-like surveys and their combinations, using both Fisher analyses and MCMC on mock data, and maps these constraints into the $(m_\chi, \langle\sigma v\rangle)$ plane for representative annihilation channels. In Sec. V we discuss the information carried by B -mode polarization and quantify its impact on bounds relative to E -mode-dominated constraints. We summarize our main conclusions and discuss implications for future CMB polarization efforts in Sec. VI, with priors, numerical details, and full posterior distributions included in the appendices.

II. CONSTRAINING POWER

CMB constraints on DM annihilation are conveniently expressed in terms of the model-independent parameter p_{ann} [4]:

$$p_{\text{ann}} \equiv f_{\text{eff}} \frac{\langle\sigma v\rangle}{m_\chi}, \quad (1)$$

where f_{eff} encodes the fraction of injected energy that is efficiently deposited into the medium, $\langle\sigma v\rangle$ is the thermally averaged cross section, and m_χ is the DM particle mass [5, 15]. For WIMP annihilation, the CMB is primarily sensitive to the overall amplitude of the energy deposition curve rather than its detailed redshift dependence. As a result, a single parameter f_{eff} accurately captures the impact of a given final state, allowing bounds on p_{ann} to be easily translated to any annihilation channel of interest [18].

DM annihilation injects energetic particles that heat and ionize the neutral intergalactic medium (IGM) [18]. The dominant impact on the CMB is an increase in the free-electron fraction $x_e(z)$, which broadens the visibility function and adds an effective optical depth $\Delta\tau_{\text{inj}}$ between recombination and reionization. To leading order, this multiplies the small-scale anisotropies by [33, 38]

$$C_\ell^{TT,EE} \rightarrow e^{-2\Delta\tau_{\text{inj}}} C_\ell^{TT,EE}, \quad (2)$$

producing a damping of the TT/EE tails that is strongly degenerate with shifts in amplitude A_s and tilt n_s of the scalar power spectrum. This suppression is evident in the top and middle panels of Fig. 1.

Annihilation also enhances large-scale polarization by generating additional E -modes through Thomson scattering, yielding a broad bump in the EE spectrum for $\ell \lesssim 100$ (top panel) [3, 5, 33]. Unlike a pure change in τ_{reio} , this feature reflects energy deposition over a wide redshift range and has a distinct ℓ -dependence, which helps to break parameter degeneracies [33].

To localize where the sensitivity to p_{ann} originates, we compute the Fisher information as a function of the multipole range under two benchmark survey models: an ‘‘Optimistic noise’’ instrument (i.e., white noise, $1'$ FWHM, $\Delta_T = 1 \mu\text{K arcmin}$ with $\Delta_P = \sqrt{2} \Delta_T$, $f_{\text{sky}} = 0.7$) and, for reference, a CVL survey with the same f_{sky} . In the bottom panel of Fig. 1 we vary a transition multipole ℓ_{min} that controls a hybrid noise model: for $\ell < \ell_{\text{min}}$ we replace the Planck noise with the Optimistic (or CVL) noise, while for $\ell \geq \ell_{\text{min}}$ we retain Planck noise levels. Thus moving ℓ_{min} to smaller values progressively upgrades more large-scale modes. The resulting forecasted 2σ upper limit on p_{ann} tightens rapidly as ℓ_{min} drops from ~ 300 to ~ 20 , with continued (but slower) improvement down to reionization scales. The near coincidence of the TT+EE and EE-only curves shows that, after marginalizing parameter degeneracies, the gain comes almost entirely from large-scale E -modes; by contrast, extending to higher ℓ yields only marginal additional benefit beyond Planck.

III. UPDATED BOUNDS

While Planck provided a nearly full-sky measurement of the CMB temperature and polarization anisotropies with unprecedented precision on large angular scales [39], recent ground-based CMB experiments have extended sensitivity to smaller scales. The Atacama Cosmology Telescope (ACT), located in the Atacama Desert, has delivered the most precise measurements of the temperature power spectrum at multipoles $\ell > 1800$, and of the E -mode polarization spectrum for $\ell > 750$ [40–42]. The South Pole Telescope (SPT)-3G, located at the South Pole, offers sensitivity competitive with ACT between $\ell = [1800, 4000]$ for the EE spectrum, and between $\ell = [2200, 4000]$ for the TE spectrum [43].

Since DM annihilation has an effect on the damping tail of both the TT and EE spectra (though to a smaller extent compared to large-scale polarization), we reassess current bounds in the post-Planck era by combining Planck with ground-based measurements that provide enhanced high- ℓ sensitivity.

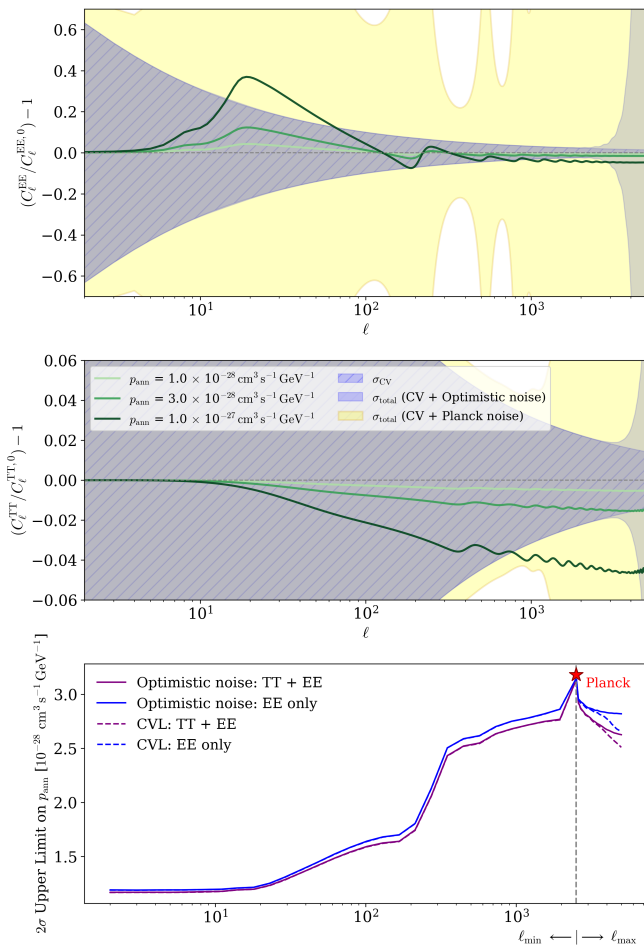


FIG. 1. **Top:** Fractional impact of varying p_{ann} on the EE and TT spectra. Outer shaded bands indicate cosmic variance + instrumental noise, and inner shaded bands indicate cosmic variance alone; both are computed for the highest value of p_{ann} ($1.0 \times 10^{-27} \text{ cm}^3 \text{ s}^{-1} \text{ GeV}^{-1}$). **Middle:** Same as middle panel but for the TT power spectrum. **Bottom:** Forecasted 2σ upper limits on p_{ann} for different experimental configurations and multipole ranges included in the Fisher analysis. Solid curves include TT+EE; dashed curves include EE-only. A Planck-like experiment with $\ell_{\text{max}} = 2500$ is taken as a baseline (marked by star).

A. Datasets

As Planck remains the most sensitive experiment at large angular scales, we combine recent datasets with Planck to maximize their joint sensitivity. Details of these combinations are given in Table I.

In adding ACT, we use the P-ACT combination as described in [42], which includes multipole cuts designed to optimize the joint constraining power of Planck and ACT while minimizing overlap. In combining with SPT, we assume that both Planck and ACT are sufficiently uncorrelated with SPT to justify adding SPT without any multipole range cuts, justified by the minimal sky overlap between SPT and other experiments [43]. We

additionally assume the ACT and SPT lensing data are sufficiently uncorrelated to be directly combined [43].

We also consider the effect of including recent DESI DR2 baryon acoustic oscillation (BAO) measurements. Supernova (SN) data are omitted, as they constrain late-time expansion rather than the early-Universe physics relevant for energy injection constraints [15, 42, 44].

B. Methodology

We use the Boltzmann solver code CLASS [45] to compute theoretical power spectra, and the Markov Chain Monte Carlo (MCMC) sampler Cobaya to explore the posterior distribution of the cosmological parameters [46, 47]. In our analysis, we vary the six standard Λ CDM parameters ($\{A_s, n_s, \theta_s, \tau_{\text{reio}}, \Omega_b h^2, \Omega_c h^2\}$), with fiducial values fixed by Planck [39], and include the annihilation parameter p_{ann} as an additional degree of freedom.

The impact of DM annihilation is modeled as an additional energy injection term that affects the recombination history, implemented through the built-in parameterization of energy deposition in CLASS [45], built on ExoCLASS [48].

To ensure convergence, we run multiple independent chains and require a Gelman-Rubin convergence criterion of $R - 1 < 0.01$ [49]. All chains use a flat prior on $p_{\text{ann}} \geq 0$, and flat priors on all cosmological parameters, provided in Table IV.

C. Results

Our results are reported in Table I, with the triangle plot showing pairwise marginalized posteriors in the Appendix. In Section IV D, we interpret the most stringent results for relevant annihilation channels and compare them to existing astronomical limits. We find that the most constraining combination is Planck + SPT; the addition of SPT tightens the bound by approximately 10%, compared to Planck alone. The addition of ACT data slightly weakens the bound, and the addition of DESI DR2 BAO data produces no statistically significant improvement. This is explained by a marginal shift away from zero in the p_{ann} posterior peak when combining ACT and Planck data (see, e.g., Fig. 33 of [42], and the discussion therein).

We obtain a slightly weaker bound for Planck-only than the official Planck 2018 result. We attribute this to our use of the SRoll2 low- ℓ likelihood, which incorporates improved systematics and map-making. When we substitute the original Planck low- ℓ likelihood, we recover the 2018 bound of $3.2 \times 10^{-28} \text{ cm}^3 \text{ s}^{-1} \text{ GeV}^{-1}$, a difference of $\sim 15\%$. This difference highlights the significant role of low- ℓ polarization data, where improved systematics have a dominant effect on the p_{ann} constraint compared to the addition of high- ℓ data.

Our results are consistent with previous analyses that indicate that most of the available constraining power will come from improved measurements of large-scale polarization [3, 18, 33].

IV. PROJECTED BOUNDS

Future satellite missions will surpass Planck in sensitivity to large-scale polarization, providing full-sky, low-noise observations at the multipoles most sensitive to energy injection. Ground-based experiments such as the Simons Observatory will contribute complementary small-scale measurements, but remain limited due to low sky coverage and poor sensitivity to low- ℓ modes compared to satellite missions. We present forecasts on p_{ann} considering multiple experimental scenarios, comparing results from Fisher-matrix calculations and MCMC analyses.

A. Future CMB Surveys

A new generation of CMB experiments will improve upon Planck's sensitivity both through better angular resolution and through lower noise across a wide range of multipoles:

a. LiteBIRD. LiteBIRD is a JAXA-led satellite mission scheduled for launch in the 2030s, with a primary science goal of detecting primordial gravitational waves via large-scale B-mode polarization [50]. The large sky coverage ($f_{\text{sky}} \gtrsim 0.7$) and strong control over systematics make LiteBIRD especially valuable for low- ℓ polarization measurements, which are highly sensitive to changes in the ionization history from DM annihilation. In contrast to ground-based experiments, LiteBIRD's space-based platform avoids atmospheric noise and allows access to the reionization bump at $\ell \lesssim 10$, where Planck noise remains a limiting factor [50, 51].

b. CMB-S4 (concept). Although the CMB-S4 program has been largely defunded, we treat it here as a representative high-resolution ground-based experiment for comparative purposes [34, 52]. The CMB-S4 concept called for an array of telescopes at the South Pole and in the Atacama Desert, with combined sensitivities approaching $\sim 1 \mu\text{K-arcmin}$ in temperature [53]. For DM annihilation, such high-resolution data primarily improve constraints via the damping tail of the CMB power spectra ($\ell \gtrsim 1000$).

c. Simons Observatory. The Simons Observatory (SO), currently operating in the Atacama Desert, will serve as the next major high-resolution ground-based CMB experiment. SO involves a combination of large- and small-aperture telescopes to target both large- and small-scale anisotropies, with a particular emphasis on high- ℓ measurements of temperature and E-mode polarization [54, 55].

B. Methodology

1. Noise Modeling

We model each frequency channel i with a Gaussian beam of full width at half maximum θ_i^{FWHM} (in radians) and white noise levels $\Delta_{T,i}$ and $\Delta_{P,i}$ (in $\mu\text{K-arcmin}$). The corresponding beam dispersion and window function are given as [56]:

$$\sigma_i = \frac{\theta_i^{\text{FWHM}}}{\sqrt{8 \ln 2}}, \quad (3)$$

$$b_{\ell,i} = \exp\left[-\frac{1}{2} \ell(\ell+1) \sigma_i^2\right]. \quad (4)$$

Map noise in $\mu\text{K-arcmin}$ is converted to $\mu\text{K-radian}$ via

$$\sigma_{X,i} = \Delta_{X,i} \times \left(\frac{\pi}{180 \times 60}\right), \quad X \in \{T, P\}. \quad (5)$$

Assuming uncorrelated channels that are beam-deconvolved at the power-spectrum level, the effective noise power spectra are obtained by inverse-variance combining channels:

$$N_\ell^{TT} = \left[\sum_i \sigma_{T,i}^{-2} b_{\ell,i}^2 \right]^{-1}, \quad (6)$$

$$N_\ell^{EE} = \left[\sum_i \sigma_{P,i}^{-2} b_{\ell,i}^2 \right]^{-1}, \quad (7)$$

$$N_\ell^{TE} = 0, \quad (8)$$

where $N_\ell^{TE} = 0$ reflects the assumption of uncorrelated temperature and polarization noise. Unless experiment-specific polarization sensitivities are provided, we adopt the conventional $\Delta_{P,i} = \sqrt{2} \Delta_{T,i}$.

We provide details of the noise models for each experiment in Table II. For all experiments, we assume efficient removal of foregrounds, and note that the effect of foreground removal method has a minor but well-understood effect on the bound [36].

Due to the contamination by atmospheric fluctuations and instrumental drifts, which typically scales as $1/f$, low- ℓ noise must be modeled carefully. For modeling ground-based experiments, we replace low- ℓ measurements ($\ell < 50$) with Planck noise. To accurately represent the systematics of Planck, we include a standard boost factor of 8 on low- ℓ polarization noise [39, 53]. We validate that this factor reproduces the true Planck bounds to within 10%.

We assume LiteBIRD's rotating half-wave plates (HWP) suppress $1/f$ noise sufficiently to include modes down to $\ell = 2$ [50, 57].

Due to the dominant effect of foregrounds on the temperature spectrum for $\ell > 3000$, we include only polarization measurements in the range $\ell = [3000, 5000]$ for forecasts on ground-based experiments [31].

TABLE I. 2σ upper limits on p_{ann} for different experimental datasets

Configuration	Datasets Included	2σ Upper Limit [$10^{-28} \text{ cm}^3 \text{ s}^{-1} \text{ GeV}^{-1}$]
Planck Only	Planck 2018 low- ℓ TT Planck 2018 low- ℓ EE (SRoll2) Planck 2018 high- ℓ TTTEEE Planck PR4 (2020) NPIPE Lensing	3.9
Planck + SPT	<i>Planck Only</i> SPT-3G D1 Lite (TnE) MUSE lensing	3.38
Planck + ACT	<i>P-ACT</i> ACT-DR6 Lenslike	4.13
Planck + ACT + SPT	<i>P-ACT</i> SPT-3G D1 Lite (TnE) MUSE lensing ACT-DR6 Lenslike	3.73
Planck + ACT + SPT + DESI	<i>Planck + ACT + SPT</i> DESI DR2 BAO	3.70

2. Fisher Forecasting

Fisher information provides a convenient metric to estimate the precision with which model parameters can be constrained. The associated covariance matrix is given as [9]:

$$\Sigma_\ell = \frac{2}{(2\ell + 1)f_{\text{sky}}} \times \begin{pmatrix} C_\ell^{TT} + N_\ell^{TT} & C_\ell^{TE} \\ C_\ell^{TE} & C_\ell^{EE} + N_\ell^{EE} \end{pmatrix} \quad (9)$$

Temperature and polarization measurements are assumed to be independent such that the noise of the TE cross spectrum vanishes. For a cosmic variance-limited experiment, $N_\ell^{TT} = N_\ell^{EE} = 0$. The Fisher information can then be computed as:

$$F_{ij} = \sum_\ell \left(\frac{\partial C_\ell}{\partial \alpha_i} \right)^T \cdot \Sigma_\ell^{-1} \cdot \left(\frac{\partial C_\ell}{\partial \alpha_j} \right) \quad (10)$$

where α denotes the cosmological parameters with respect to which the derivatives are taken. The derivatives are computed via finite differences with step sizes chosen to optimize numerical stability.

3. Forecasting via MCMC Sampling

To validate our Fisher forecasts, we estimate the sensitivity of future experiments using MCMC simulations drawn from Gaussian approximations to the likelihood. The likelihood is evaluated on mock data (fiducial spectra plus noise), and we assume a Wishart-distributed covariance estimator for each multipole in the specified range.

Let \hat{C}_ℓ^{XY} denote the observed (mock) power spectra and C_ℓ^{XY} the theoretical spectra, where $X, Y \in \{T, E\}$. The total covariance matrix at each multipole ℓ is given

by:

$$\mathbf{C}_\ell^{\text{theory}} = \begin{pmatrix} C_\ell^{TT} + N_\ell^{TT} & C_\ell^{TE} \\ C_\ell^{TE} & C_\ell^{EE} + N_\ell^{EE} \end{pmatrix}, \quad (11)$$

where N_ℓ^{TT} and N_ℓ^{EE} denote the noise power spectra. The corresponding matrix of mock data is given by:

$$\hat{\mathbf{C}}_\ell = \begin{pmatrix} \hat{C}_\ell^{TT} & \hat{C}_\ell^{TE} \\ \hat{C}_\ell^{TE} & \hat{C}_\ell^{EE} \end{pmatrix}. \quad (12)$$

The log-likelihood is then computed as:

$$-2 \log \mathcal{L} = f_{\text{sky}} \sum_{\ell=\ell_{\text{min}}}^{\ell_{\text{max}}} (2\ell + 1) \left[\text{Tr}(\hat{\mathbf{C}}_\ell \mathbf{C}_\ell^{-1}) - \log \det(\hat{\mathbf{C}}_\ell \mathbf{C}_\ell^{-1}) - 2 \right]. \quad (13)$$

We use **Cobaya** to sample from the mock likelihoods, using the same parameterization and convergence criteria described in Section III B.

C. Dataset Combinations

We evaluate several forecast configurations that combine different experiments across complementary multipole ranges, chosen to maximize joint sensitivity (see Table II). For each configuration, we construct hybrid spectra by selecting the experiment with the best expected performance in the relevant ℓ range:

- **CMB-S4 + Planck:**

- $\ell < 50$: Planck
- $\ell \in [50, 3000]$: CMB-S4 TT, TE, EE
- $\ell \in [3000, 5000]$: CMB-S4 EE-only

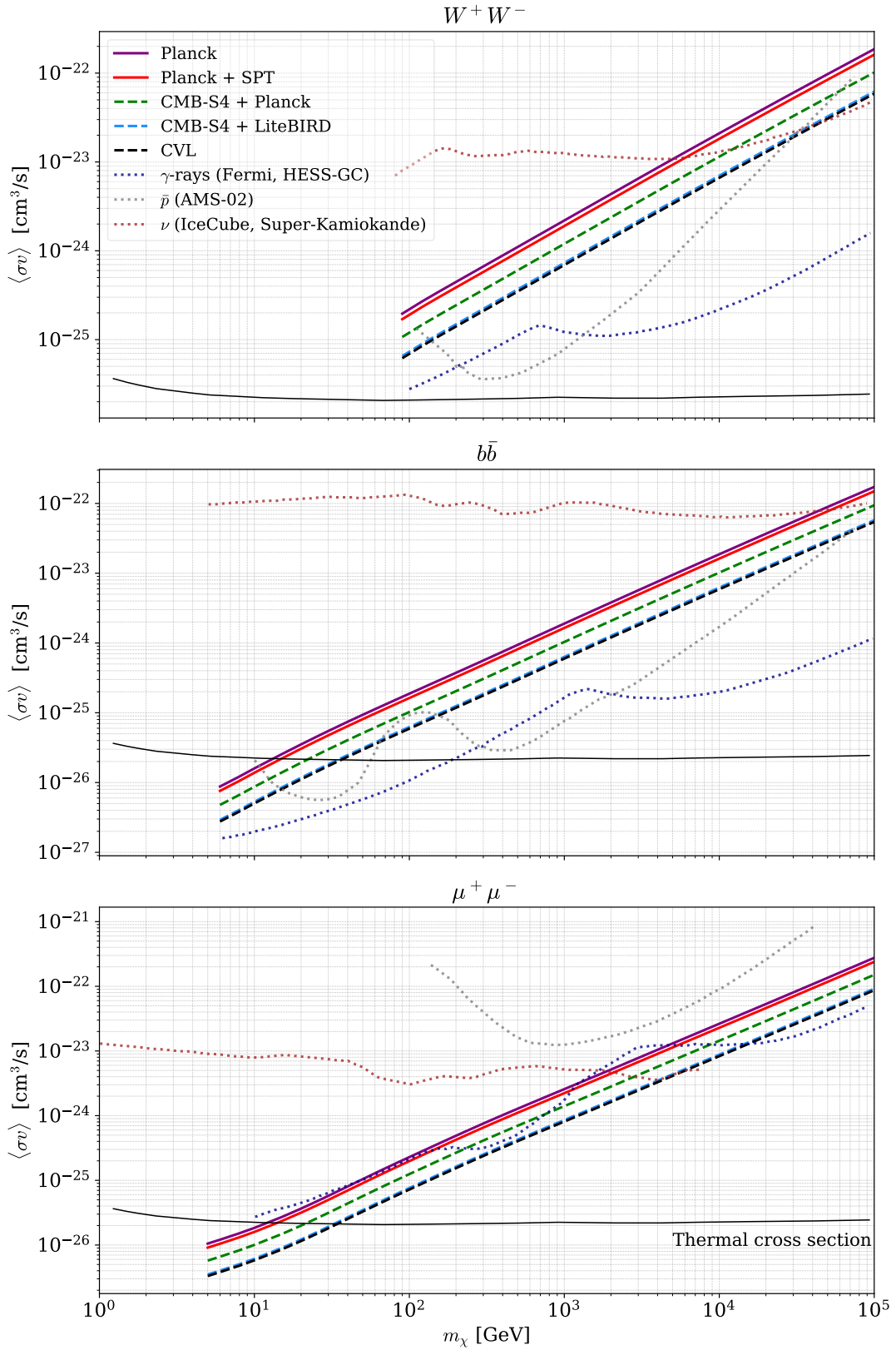


FIG. 2. Projected 2σ upper bounds on the DM annihilation cross section $\langle\sigma v\rangle$ as a function of DM mass m_χ for three annihilation channels: W^+W^- (top), $b\bar{b}$ (middle), and $\mu^+\mu^-$ (bottom). The channel-dependent f_{eff} curves used to convert constraints on p_{ann} to $\langle\sigma v\rangle$ are taken from Ref. [15]. Solid lines show current CMB constraints derived in this work for Planck and Planck + SPT; dashed lines show projected bounds for CMB-S4 + Planck, CMB-S4 + LiteBIRD, and a CVL experiment. Dotted lines indicate complementary limits from indirect detection, extrapolated from [22] (see also references therein). We also show the thermal cross section as a function of DM mass [58].

TABLE II. Experimental configurations (beam widths and noise levels per frequency channel) used in the forecasts. Where polarization noise is not provided, we adopt the standard $\Delta_P = \sqrt{2} \Delta_T$.

Experiment	ν [GHz]	Beam FWHM [arcmin]	Δ_T (Δ_P) [μ K-arcmin]	f_{sky}	ℓ -range
Planck [39]	100	10.0	65 (103)	0.7	$2 < \ell < 2500$
	143	7.0	43 (81)		
	217	5.0	66 (134)		
CMB-S4 [31, 53]	–	1.0	1.0	0.4	T: $50 < \ell < 3000$ P: $50 < \ell < 5000$
Simons Observatory [54]					
<i>Small Aperture Telescopes</i>	27	91	35	0.7	$50 < \ell < 5000$
	39	63	21		
	93	30	2.6		
	145	17	3.3		
	225	11	6.3		
	280	9	16		
	27	7.4	71		
<i>Large Aperture Telescopes</i>	39	5.1	36	0.2	$50 < \ell < 5000$
	93	2.2	8		
	145	1.4	10		
	225	1.0	22		
	280	0.9	53		
LiteBIRD [50]	40	70.5	26.46	0.7	$2 \leq \ell \leq 200$
	50	58.5	23.66		
	60	51.1	15.07		
	68	41.6, 47.1	14.08, 22.47		
	78	36.9, 43.8	11.00, 13.53		
	89	33.0, 41.5	8.68, 20.34		
	100	30.2, 37.8	7.31, 6.00		
	119	26.3, 33.6	5.44, 4.03		
	140	23.7, 30.8	5.13, 4.51		
	166	28.9	3.94		
	195	28.0, 28.6	4.99, 7.43		
	235	24.7	7.63		
	280	22.5	9.76		
	337	20.9	15.52		
	402	17.9	33.55		

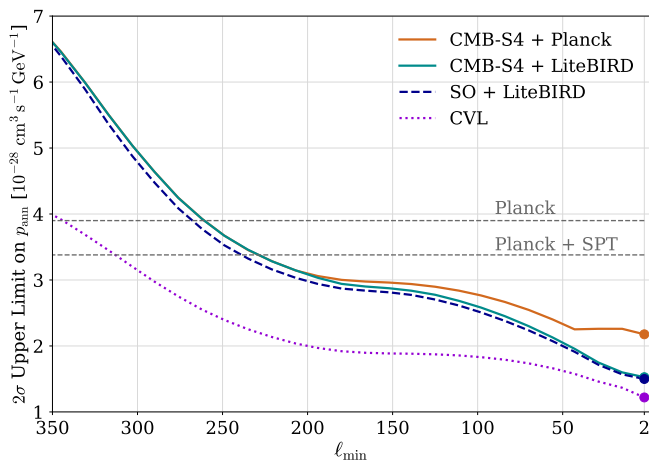


FIG. 3. Fisher-forecasted 2σ upper limit on p_{ann} as a function of the minimum multipole ℓ_{min} included in the analysis. For $\ell > 200$, forecasts assume either a CMB-S4-like experiment (solid lines), or a Simons Observatory-like configuration for *Simons + LiteBIRD* (purple dashed); see Table II for configuration details. For $\ell < 200$, each forecast uses the low- ℓ experiment indicated in the legend. The CVL forecast (dotted) assumes coverage of $f_{\text{sky}} = 0.7$ and sensitivity over the entire multipole range up to $\ell = 5000$, without imposing any ℓ_{min} cut. Horizontal dashed lines refer to bounds computed in this work (see Table I).

- **CMB-S4 + LiteBIRD:**

- $\ell < 200$: LiteBIRD
- $\ell \in [200, 3000]$: CMB-S4 TT,TE,EE
- $\ell \in [3000, 5000]$: CMB-S4 EE-only

- **SO + LiteBIRD:**

- $\ell < 200$: LiteBIRD
- $\ell \in [200, 3000]$: SO TT,TE,EE
- $\ell \in [3000, 5000]$: SO EE-only

- **CVL:**

- $\ell \in [2, 5000]$: TT,TE,EE with $N_\ell = 0$ for all spectra

D. Results

Table III summarizes our Fisher forecast results. As a validation, we check that the Fisher and MCMC pipelines produce bounds that agree within 20% across all configurations (see Table III). Given the greater robustness of MC sampling, we report the MC results for all further analysis.

Relative to the Planck-only constraint in Table I ($3.9 \times 10^{-28} \text{ cm}^3 \text{ s}^{-1} \text{ GeV}^{-1}$), adding a high-resolution ground-based experiment (CMB-S4-like) tightens the 2σ upper limit to $2.13 \times 10^{-28} \text{ cm}^3 \text{ s}^{-1} \text{ GeV}^{-1}$, which corresponds

to a $\simeq 46\%$ improvement. Including LiteBIRD data yields $1.30 \times 10^{-28} \text{ cm}^3 \text{ s}^{-1} \text{ GeV}^{-1}$, which gives an additional $\simeq 38\%$ improvement beyond CMB-S4+Planck and $\simeq 67\%$ relative to Planck alone. A Simons+LiteBIRD configuration yields $1.27 \times 10^{-28} \text{ cm}^3 \text{ s}^{-1} \text{ GeV}^{-1}$, which lies within $\sim 3\%$ of the CMB-S4+LiteBIRD bound, indicating that once large-scale polarization is near cosmic variance, further high- ℓ noise reduction brings only marginal gains. The Simons+LiteBIRD combination effectively saturates (to within $\sim 4\%$) the constraint of a CVL experiment with equivalent sky coverage ($f_{\text{sky}} = 0.7$).

Figure 3 shows how the bound varies with the minimum multipole ℓ_{min} included in the analysis. The constraint improves most rapidly as progressively more intermediate multipoles are added, reflecting the fact that these scales carry significant sensitivity to energy injection. For $\ell_{\text{min}} < 200$, we also illustrate the effect of replacing Planck low- ℓ noise with LiteBIRD’s higher-sensitivity measurements: doing so yields a noticeable tightening of the limit beyond what is possible with Planck low- ℓ noise, demonstrating the additional constraining power that comes from improved large-scale polarization. These trends are consistent with previous analyses that identify large-scale polarization as a key limiting factor for energy injection constraints [3, 15, 33].

In Figure 2, we map the constraints on p_{ann} into the $m_\chi - \langle \sigma v \rangle$ plane using the appropriate f_{eff} values for three representative annihilation channels and compare them to existing astrophysical bounds.

The resulting projections show that, for hadronic and gauge-boson (bb and W^+W^-) channels, the improvement provided by future experiments will not provide a more stringent bound with respect to the astronomical ones (based on the non-observation of excess gamma rays from dwarf galaxies and the Galactic center).

If the $\mu^+\mu^-$ channel is considered, the constraining power of future experiments will achieve the most stringent bound up to $\simeq 10$ TeV. However, in any annihilation channel under consideration, the *thermal WIMP* paradigm will not be probed at masses larger than $\simeq 30$ GeV, contrary to some previous claims.

TABLE III. Forecasted 2σ upper limits on p_{ann} , comparing two forecasting methods: MCMC (see IV B 3), and Fisher forecasting (see IV B 2).

Experiment	2σ upper limit [$10^{-28} \text{ cm}^3 \text{ s}^{-1} \text{ GeV}^{-1}$]	
	MCMC	Fisher
CMB-S4 + Planck	2.13	2.11
CMB-S4 + LiteBIRD	1.30	1.52
SO + LiteBIRD	1.27	1.49
CVL	1.23	1.25

V. EFFECT OF TENSOR MODES

Future CMB surveys will measure the B-mode power spectrum with far greater precision than previous datasets, motivating the question of whether BB contributes meaningful additional information to DM annihilation constraints. In the absence of primordial tensor modes ($r = 0$), all B-mode power arises from gravitational lensing, which converts E-modes into B-modes. Any modification to the large-scale E-mode signal induced by energy injection is therefore partially remapped into B. If primordial tensors are present, they add BB power on the same large angular scales ($\ell \lesssim 10$) that carry most of the annihilation leverage.

We assess the impact of including BB through a Fisher analysis, in which we consider only two-point CMB power spectra and do not include a separate Fisher contribution from lensing reconstruction (e.g., the $\phi\phi$ power spectrum). As a result, any improvement from adding BB reflects the incremental lensing information contained in the B-mode power spectrum within a two-point, Gaussian approximation.

Within this framework, we extend the covariance matrix in Eq. 9 to include a diagonal B-mode block [59, 60]:

$$\Sigma_{\ell}^{(TEB)} = \frac{2}{(2\ell + 1)f_{\text{sky}}} \times \begin{pmatrix} C_{\ell}^{TT} + N_{\ell}^{TT} & C_{\ell}^{TE} & 0 \\ C_{\ell}^{TE} & C_{\ell}^{EE} + N_{\ell}^{EE} & 0 \\ 0 & 0 & C_{\ell}^{BB} + N_{\ell}^{BB} \end{pmatrix}, \quad (14)$$

where C_{ℓ}^{BB} is the lensed BB spectrum. We assume no delensing, equal polarization noise ($N_{\ell}^{BB} \equiv N_{\ell}^{EE}$), and vanishing TB and EB correlations [60].

We quantify the incremental value of BB by comparing Fisher constraints using TT, TE, EE versus TT, TE, EE, BB for the same experiment and ℓ -range, in the following configurations:

a. *CVL*. For a CVL survey with $f_{\text{sky}} = 0.7$ and $\ell_{\text{max}} = 3000$, adding *BB* tightens the 2σ upper limit on p_{ann} by 5.5% relative to the TT, TE, EE baseline.

b. *LiteBIRD*. For a more realistic experiment, we consider a LiteBIRD-only experiment as described in Table II. Including BB tightens the upper limit by 1.5%; the minor gain is concentrated at the very largest scales ($\ell < 10$), where the leverage there is already dominated by E-modes.

We also repeat these forecasts with fixed primordial tensors, $r = 10^{-3}$. Including BB tightens the p_{ann} bounds by 5.5% for a CVL survey and 1.7% for LiteBIRD—numerically similar to the $r = 0$ case—indicating that small tensor contributions do not enhance sensitivity to p_{ann} . The BB response is dominated by gravitational lensing of the E-modes: energy injection alters EE (via an increased free-electron fraction and a broadened visibility function), and lensing remaps those changes into B-modes. Consequently, BB carries little

independent information once EE and TE are included, yielding at most marginal additional constraining power; the sensitivity is effectively captured by large-scale E-mode polarization [59].

For an idealized LiteBIRD-like experiment, the incremental leverage from BB remains at the percent level, with any gain concentrated on scales $\ell \lesssim 10$ where EE already dominates. Realistic delensing and noise modeling would further reduce the BB contribution. We therefore view BB primarily as a useful internal consistency check on the polarization signature of energy injection, rather than a significant contribution to the p_{ann} constraint.

VI. DISCUSSION AND CONCLUSIONS

Our analysis isolates the multipole ranges and experimental features that most directly govern CMB sensitivity to annihilating dark matter. Two main conclusions emerge. First, present constraints are already limited primarily by large-scale E-mode polarization; adding high- ℓ temperature and polarization from ground-based experiments (ACT/SPT or a CMB-S4-like survey) provides only modest gains once the low- ℓ polarization uncertainty is fixed. Second, forecasts that include a space-based mission with precise low- ℓ measurements (LiteBIRD) approach the cosmic-variance limit for $f_{\text{sky}} \simeq 0.7$, with only marginal improvement from further reducing high- ℓ noise. Taken together, these trends reinforce the picture that the injected-energy signal acts mainly as an effective additional optical depth, enhancing large-scale polarization and thereby making low- ℓ sensitivity—not high- ℓ resolution—the primary driver of constraining power.

Near-term progress hinges on improved large-scale polarization: absolute calibration, polarization-angle systematics, $1/f$ suppression, and robust foreground control. A LiteBIRD-like survey paired with current or next-generation ground data effectively saturates the information available to the CMB for annihilation histories of the type modeled here. The CMB remains a uniquely clean, model-agnostic bound on annihilation, with forthcoming polarization measurements poised to close the gap to the cosmic-variance floor.

ACKNOWLEDGMENTS

We would like to thank Junsong Cang and Anže Slosar for their helpful clarifications regarding their previous work. We are also grateful to Giovanni Signorelli for his comments regarding LiteBIRD sensitivity.

DA acknowledges support from the Generalitat Valenciana grant CIGRIS/2021/054, and grant PID2023-151418NB-I00, which is funded by MCIU/AEI/10.13039/501100011033/ FEDER, UE.

DG acknowledges support from the projects *Theoretical Astroparticle Physics (TAsP)* and *TEONGRAV* funded by INFN.

CM acknowledges support from the MIT International Science and Technology Initiatives (MISTI), which funded her internship at the University of Pisa.

This work made use of CLASS [45], Cobaya [46, 47], `getdist` [61], `matplotlib` [62], `NumPy` [63], `SciPy` [64], `Webplotdigitizer` [65], and any dependencies.

Appendix A: Prior ranges

TABLE IV. Flat prior ranges assumed for the cosmological parameters in our analysis.

Parameter	Prior
p_{ann} [$\text{cm}^3 \text{s}^{-1} \text{GeV}^{-1}$]	[0, 3×10^{-27}]
n_s	[0.9, 1.1]
τ_{reio}	[0, 0.1]
$\log(10^{10} A_s)$	[2.6, 3.5]
$\Omega_b h^2$	[0.017, 0.027]
$\Omega_c h^2$	[0.09, 0.15]
H_0 [km/s/Mpc]	[60, 80]

In Table IV we give the prior ranges assumed for the cosmological parameters in our analysis.

Appendix B: Triangle plot

In Fig. 4 we show the joint posterior distributions for p_{ann} and the standard six Λ CDM parameters obtained from various combinations of CMB datasets in Section III C. The addition of high-resolution ground-based measurements (ACT and SPT) to Planck data slightly tightens the constraints on all parameters, most notably p_{ann} . Cross-correlations between p_{ann} and the recombination parameters τ_{reio} , n_s , and $\log(10^{10} A_s)$ are significantly reduced once ACT+SPT data are included, reflecting the improved polarization sensitivity at both large and small scales. The parameters $\Omega_b h^2$ and $\Omega_c h^2$ remain almost stable across data combinations, while H_0 shows only minor shifts, consistent with expectations that energy-injection constraints primarily affect the ionization and primordial-spectrum sectors.

-
- [1] G. Arcadi, M. Dutra, P. Ghosh, M. Lindner, Y. Mambrini, M. Pierre, S. Profumo, and F. S. Queiroz, *Eur. Phys. J. C* **78**, 203 (2018), arXiv:1703.07364 [hep-ph].
- [2] J. A. Adams, S. Sarkar, and D. W. Sciama, *Mon. Not. Roy. Astron. Soc.* **301**, 210 (1998), arXiv:astro-ph/9805108.
- [3] N. Padmanabhan and D. P. Finkbeiner, *Phys. Rev. D* **72**, 023508 (2005).
- [4] S. Galli, F. Iocco, G. Bertone, and A. Melchiorri, *Phys. Rev. D* **80**, 023505 (2009), arXiv:0905.0003 [astro-ph.CO].
- [5] T. R. Slatyer, N. Padmanabhan, and D. P. Finkbeiner, *Phys. Rev. D* **80**, 043526 (2009), arXiv:0906.1197 [astro-ph.CO].
- [6] T. Kanzaki, M. Kawasaki, and K. Nakayama, *Prog. Theor. Phys.* **123**, 853 (2010), arXiv:0907.3985 [astro-ph.CO].
- [7] G. Hutsi, J. Chluba, A. Hektor, and M. Raidal, *Astron. Astrophys.* **535**, A26 (2011), arXiv:1103.2766 [astro-ph.CO].
- [8] S. Galli, F. Iocco, G. Bertone, and A. Melchiorri, *Phys. Rev. D* **84**, 027302 (2011), arXiv:1106.1528 [astro-ph.CO].
- [9] D. P. Finkbeiner, S. Galli, T. Lin, and T. R. Slatyer, *Phys. Rev. D* **85**, 043522 (2012), arXiv:1109.6322 [astro-ph.CO].
- [10] G. Giesen, J. Lesgourgues, B. Audren, and Y. Ali-Haïmoud, *JCAP* **12**, 008, arXiv:1209.0247 [astro-ph.CO].
- [11] J. M. Cline and P. Scott, *JCAP* **03**, 044, [Erratum: *JCAP* **05**, E01 (2013)], arXiv:1301.5908 [astro-ph.CO].
- [12] C. Weniger, P. D. Serpico, F. Iocco, and G. Bertone, *Phys. Rev. D* **87**, 123008 (2013), arXiv:1303.0942 [astro-ph.CO].
- [13] L. Lopez-Honorez, O. Mena, S. Palomares-Ruiz, and A. C. Vincent, *JCAP* **07**, 046, arXiv:1303.5094 [astro-ph.CO].
- [14] R. Diamanti, L. Lopez-Honorez, O. Mena, S. Palomares-Ruiz, and A. C. Vincent, *JCAP* **02**, 017, arXiv:1308.2578 [astro-ph.CO].
- [15] M. S. Madhavacheril, N. Sehgal, and T. R. Slatyer, *Physical Review D* **89**, 10.1103/physrevd.89.103508 (2014).
- [16] S. Galli, T. R. Slatyer, M. Valdes, and F. Iocco, *Phys. Rev. D* **88**, 063502 (2013), arXiv:1306.0563 [astro-ph.CO].
- [17] P. A. R. Ade *et al.* (Planck), *Astron. Astrophys.* **594**, A13 (2016), arXiv:1502.01589 [astro-ph.CO].
- [18] T. R. Slatyer, *Phys. Rev. D* **93**, 023527 (2016), arXiv:1506.03811 [hep-ph].
- [19] T. R. Slatyer, *Phys. Rev. D* **93**, 023521 (2016), arXiv:1506.03812 [astro-ph.CO].
- [20] T. R. Slatyer and C.-L. Wu, *Phys. Rev. D* **95**, 023010 (2017), arXiv:1610.06933 [astro-ph.CO].
- [21] M. Kawasaki, H. Nakatsuka, K. Nakayama, and T. Sekiguchi, *JCAP* **12** (12), 015, arXiv:2105.08334 [astro-ph.CO].
- [22] M. Cirelli, A. Strumia, and J. Zupan, arXiv e-prints, arXiv:2406.01705 (2024), arXiv:2406.01705 [hep-ph].
- [23] P. J. E. Peebles, S. Seager, and W. Hu, *Astrophys. J. Lett.* **539**, L1 (2000), arXiv:astro-ph/0004389.
- [24] R. Bean, A. Melchiorri, and J. Silk, *Phys. Rev. D* **68**, 083501 (2003).
- [25] A. G. Doroshkevich, I. P. Naselsky, P. D. Naselsky, and I. D. Novikov, *Astrophys. J.* **586**, 709 (2003), arXiv:astro-ph/0208114.
- [26] X.-L. Chen and M. Kamionkowski, *Phys. Rev. D* **70**, 043502 (2004), arXiv:astro-ph/0310473.

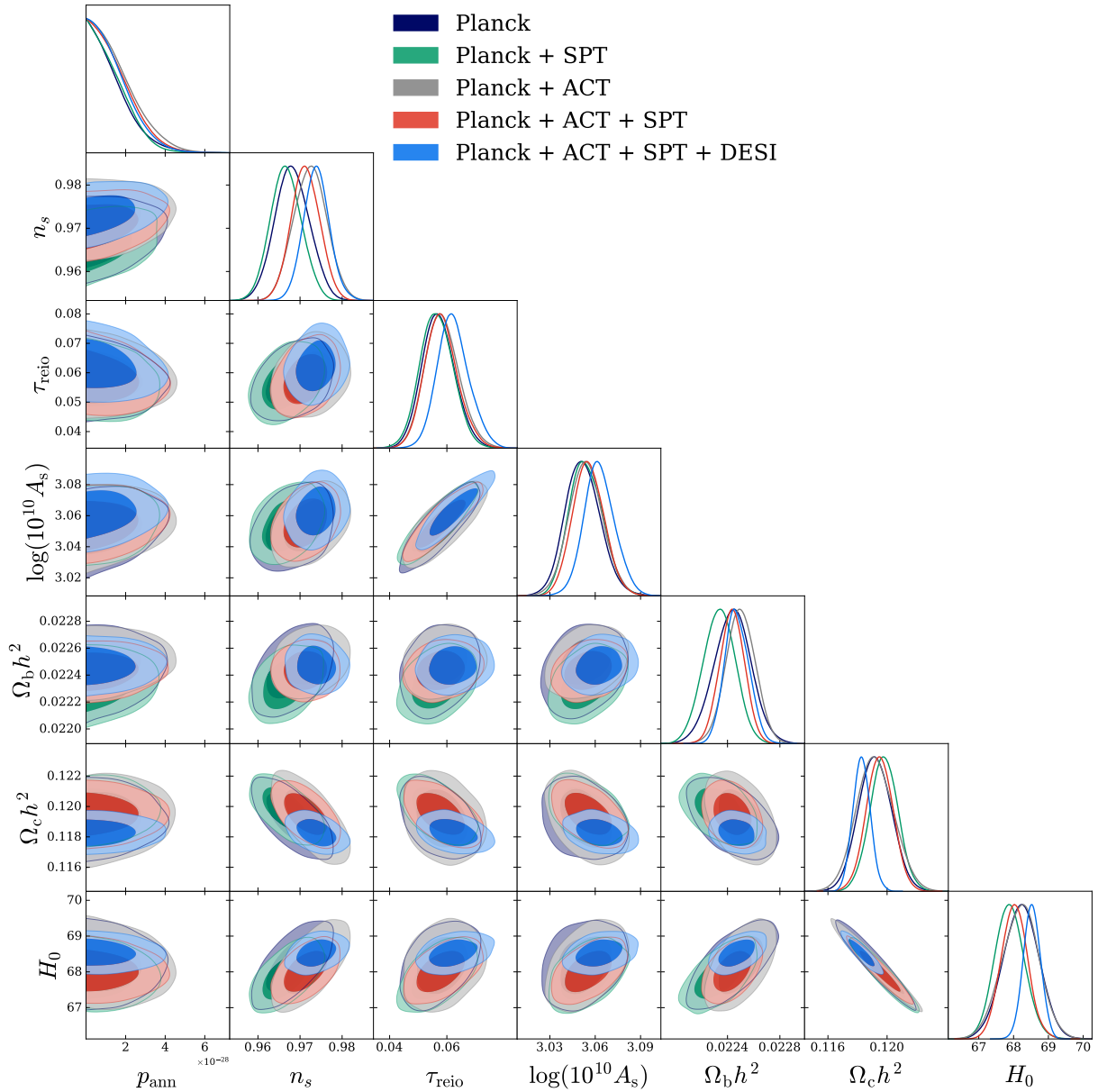


FIG. 4. Joint posteriors for $\{p_{\text{ann}}, n_s, \tau_{\text{reio}}, \log(10^{10} A_s), \Omega_b h^2, \Omega_c h^2, H_0\}$ from updated data combinations (see Table I). Shaded regions denote 68% and 95% credible intervals; diagonal panels show the corresponding 1D marginals.

- [27] S. H. Hansen and Z. Haiman, *Astrophys. J.* **600**, 26 (2004), [arXiv:astro-ph/0305126](#).
- [28] E. Pierpaoli, *Phys. Rev. Lett.* **92**, 031301 (2004), [arXiv:astro-ph/0310375](#).
- [29] S. Galli, M. Martinelli, A. Melchiorri, L. Pagano, B. D. Sherwin, and D. N. Spergel, *Phys. Rev. D* **82**, 123504 (2010), [arXiv:1005.3808 \[astro-ph.CO\]](#).
- [30] S. Galli, K. Benabed, F. Bouchet, J.-F. Cardoso, F. Elsner, E. Hivon, A. Mangilli, S. Prunet, and B. Wandelt, *Phys. Rev. D* **90**, 063504 (2014), [arXiv:1403.5271 \[astro-ph.CO\]](#).
- [31] W. L. K. Wu, J. Errard, C. Dvorkin, C. L. Kuo, A. T. Lee, P. McDonald, A. Slosar, and O. Zahn, *The Astrophysical Journal* **788**, 138 (2014).
- [32] E. Calabrese, D. Alonso, and J. Dunkley, *Phys. Rev. D* **95**, 063504 (2017), [arXiv:1611.10269 \[astro-ph.CO\]](#).
- [33] D. Green, P. D. Meerburg, and J. Meyers, *Journal of Cosmology and Astroparticle Physics* **2019** (04), 025.
- [34] K. N. Abazajian *et al.* (CMB-S4), *CMB-S4 Science Book, First Edition* (2016) [arXiv:1610.02743 \[astro-ph.CO\]](#).
- [35] J. Cang, Y. Gao, and Y.-Z. Ma, *Phys. Rev. D* **102**, 103005 (2020).
- [36] Z.-X. Zhang, Y.-M. Wang, J. Cang, Z. Zhang, Y. Liu, S.-Y. Li, Y. Gao, and H. Li, *Journal of Cosmology and Astroparticle Physics* **2023** (10), 002.
- [37] Y.-N. Wang, X.-C. Duan, T.-P. Tang, Z. Wang, and Y.-L. S. Tsai, *JCAP* **08**, 059, [arXiv:2502.18263 \[hep-ph\]](#).
- [38] A. Natarajan, *Physical Review D* **85**, 10.1103/physrevd.85.083517 (2012).

- [39] N. Aghanim *et al.* (Planck), *Astron. Astrophys.* **641**, A6 (2020), [Erratum: *Astron. Astrophys.* 652, C4 (2021)], [arXiv:1807.06209](https://arxiv.org/abs/1807.06209) [astro-ph.CO].
- [40] S. Naess *et al.* (Atacama Cosmology Telescope), *JCAP* **11**, 061, [arXiv:2503.14451](https://arxiv.org/abs/2503.14451) [astro-ph.CO].
- [41] T. Louis *et al.* (Atacama Cosmology Telescope), *JCAP* **11**, 062, [arXiv:2503.14452](https://arxiv.org/abs/2503.14452) [astro-ph.CO].
- [42] E. Calabrese *et al.* (Atacama Cosmology Telescope), *JCAP* **11**, 063, [arXiv:2503.14454](https://arxiv.org/abs/2503.14454) [astro-ph.CO].
- [43] E. Camphuis *et al.* (SPT-3G), SPT-3G D1: CMB temperature and polarization power spectra and cosmology from 2019 and 2020 observations of the SPT-3G Main field (2025), [arXiv:2506.20707](https://arxiv.org/abs/2506.20707) [astro-ph.CO].
- [44] S. Rueda-Blanco, C. Delgado-Correal, M.-A. Higuera-G., and S. Torres Arzayus, in *32nd General Assembly International Union (IAUGA 2024)* (2024) p. 2915.
- [45] D. Blas, J. Lesgourgues, and T. Tram, *Journal of Cosmology and Astroparticle Physics* **2011** (07), 034–034.
- [46] J. Torrado and A. Lewis, *JCAP* **05**, 057, [arXiv:2005.05290](https://arxiv.org/abs/2005.05290) [astro-ph.IM].
- [47] J. Torrado and A. Lewis, *Cobaya: Bayesian analysis in cosmology*, Astrophysics Source Code Library, record ascl:1910.019 (2019), ascl:1910.019.
- [48] P. Stöcker, M. Krämer, J. Lesgourgues, and V. Poulin, *Journal of Cosmology and Astroparticle Physics* **2018** (03), 018, [arXiv:1801.01871](https://arxiv.org/abs/1801.01871) [astro-ph, physics:hep-ph].
- [49] A. Gelman and D. B. Rubin, *Statistical Science* **7**, 10.1214/ss/1177011136 (1992).
- [50] E. Allys *et al.* (LiteBIRD), *PTEP* **2023**, 042F01 (2023), [arXiv:2202.02773](https://arxiv.org/abs/2202.02773) [astro-ph.IM].
- [51] N. Sailer, E. Castorina, S. Ferraro, and M. White, *Journal of Cosmology and Astroparticle Physics* **2021** (12), 049.
- [52] CMB-S4 Collaboration, CMB-S4: Cosmic microwave background stage-4 (official website), <https://cmb-s4.org/>, accessed: 2025-09-01.
- [53] S. Ilić *et al.* (Euclid), *Astron. Astrophys.* **657**, A91 (2022), [arXiv:2106.08346](https://arxiv.org/abs/2106.08346) [astro-ph.CO].
- [54] P. Ade *et al.* (Simons Observatory), *JCAP* **02**, 056, [arXiv:1808.07445](https://arxiv.org/abs/1808.07445) [astro-ph.CO].
- [55] N. Galitzki *et al.* (SO), *Astrophys. J. Suppl.* **274**, 33 (2024), [arXiv:2405.05550](https://arxiv.org/abs/2405.05550) [astro-ph.IM].
- [56] L. Knox, *Phys. Rev. D* **52**, 4307 (1995).
- [57] S. Micheli *et al.*, *Proc. SPIE Int. Soc. Opt. Eng.* **13102**, 131022R (2024), [arXiv:2407.15294](https://arxiv.org/abs/2407.15294) [astro-ph.IM].
- [58] G. Steigman, B. Dasgupta, and J. F. Beacom, *Phys. Rev. D* **86**, 023506 (2012), [arXiv:1204.3622](https://arxiv.org/abs/1204.3622) [hep-ph].
- [59] D. Scott, D. Contreras, A. Narimani, and Y.-Z. Ma, *Journal of Cosmology and Astroparticle Physics* **2016** (06), 046–046.
- [60] S. M. Kasanda and K. Moodley, *Journal of Cosmology and Astroparticle Physics* **2014** (12), 041–041.
- [61] A. Lewis, *JCAP* **08**, 025, [arXiv:1910.13970](https://arxiv.org/abs/1910.13970) [astro-ph.IM].
- [62] J. D. Hunter, *Computing in Science & Engineering* **9**, 90 (2007).
- [63] C. R. Harris *et al.*, *Nature* **585**, 357 (2020), [arXiv:2006.10256](https://arxiv.org/abs/2006.10256) [cs.MS].
- [64] P. Virtanen *et al.*, *Nature Meth.* **17**, 261 (2020), [arXiv:1907.10121](https://arxiv.org/abs/1907.10121) [cs.MS].
- [65] A. Rohatgi, Webplotdigitizer, <https://automeris.io>, version 5.2.